ORIGINAL PAPER

# Gd³⁺ complexes conjugated to Pittsburgh compound B: potential MRI markers of β-amyloid plaques

André F. Martins · Jean-François Morfin ·
Carlos F. G. C. Geraldes · Éva Tóth

**Abstract** In an effort towards the visualization of β-amyloid (Aβ) plaques by $T_1$-weighted magnetic resonance imaging for detection of Alzheimer's disease, we report the synthesis and characterization of stable, noncharged Gd³⁺ complexes of three different 1,4,7,10-tetraazacyclododecane-1,4,7-triacetic acid monoamide derivatives conjugated to Pittsburgh compound B, a well-established marker of Aβ plaques. The ligands $L_1$, $L_2$, and $L_3$ differ in the nature and size of the spacer linking the macrocyclic chelator and the Pittsburgh compound B targeting moiety, which affects their lipophilicity, the octanol–water partition coefficients of the complexes ranging from −0.15 to 0.32. Given their amphiphilic behavior, the complexes form micelles in aqueous solution (critical micellar concentration 1.00–1.49 mM). The parameters determining the relaxivity, including the water exchange rate and the rotational correlation times, were assessed for the monomeric and the micellar form by a combined $^{17}$O NMR and $^1$H nuclear magnetic relaxation dispersion (NMRD) study. They are largely influenced by the aggregation state and the hydrophobic character of the linkers. The analysis of the rotational dynamics for the aggregated state in terms of local and global motions using the Lipari–Szabo approach indicates highly flexible, large aggregates. On binding of the complexes to human serum albumin or to the amyloid peptide $Aβ_{1–40}$ in solution, they undergo a fourfold and a twofold relaxivity increase, respectively (40 MHz). Proton relaxation enhancement studies confirmed moderate interaction of Gd($L_1$) and Gd($L_3$) with human serum albumin, with $K_A$ values ranging between 250 and 910 M⁻¹.

**Keywords** Contrast agents · Gadolinium · Magnetic resonance imaging · Lanthanides · Amyloid peptides

A. F. Martins · J.-F. Morfin · É. Tóth (✉)
Centre de Biophysique Moléculaire,
CNRS, Université d'Orléans,
Rue Charles Sadron,
45071 Orléans Cedex 2, France
e-mail: eva.jakabtoth@cnrs-orleans.fr

A. F. Martins · C. F. G. C. Geraldes (✉)
Department of Life Sciences,
Faculty of Sciences and Technology,
University of Coimbra,
P.O. Box 3046, 3001-401 Coimbra, Portugal
e-mail: geraldes@ci.uc.pt

## Introduction

Alzheimer's disease (AD) is the chronic neurodegenerative disorder that constitutes the most frequent form of intellectual deterioration in elderly individuals [1]. It is characterized by brain deposition of amyloid plaques and neurofibrillary tangles that constitute representative neuropathological markers of this disease [2, 3]. Today, the diagnosis of AD is mainly based on cognitive tests, and it becomes definitive only in later stages of the disease, when several sections of the brain are seriously damaged and progressive cognitive decline has occurred and affected the person's ability to perform everyday activities. Although amyloid deposition is not a reliably quantitative biomarker for AD, imaging solutions based on innovative imaging probes that visualize amyloid plaques could contribute to the early identification of the disease, allowing prompt

intervention to slow the progress of the disease, even without a definitive cure being available today. They could be also of invaluable help for delineating novel therapies by facilitating drug development.

The development of in vivo imaging probes for AD has so far mainly focused on nuclear probes. Many β-amyloid (Aβ)-labeling nuclear imaging agents have been reported, mostly based on small organic compounds, such as [11]C- and ^{18}F-labeled derivatives of stilbene [4] and Pittsburgh compound B (PiB) [5, 6]. These are promising PET tracers of AD, owing to their high in vivo binding affinities for Aβ aggregates and efficient blood–brain barrier (BBB) permeation. Some of these compounds are approaching or are already in clinical application [4, 6, 7]. Their limitations are general and are mainly associated with the short lifetime of the radioisotope, the use of ionizing radiation, and the low spatial resolution of the imaging technique, although the use of co-localized PET–CT images partially alleviates this problem [8, 9]. Several small, neutral ^{99m}Tc-based Aβ binding probes for AD detection using single-photon-emission CT (SPECT) have also been reported, and some showed reasonable brain uptake and affinity towards Aβ plaques, such as those based on pyridyl benzofurane derivatives [10]. However, despite the progress in in vivo nuclear imaging of AD, there is a need for novel applications based on less invasive imaging techniques with better resolution.

MRI is a powerful clinical and biological imaging tool, offering noninvasive exploration of structure and function with excellent spatial resolution. In contrast to nuclear imaging techniques, MRI does not imply any radiation burden for the patient. The intrinsic MRI contrast can be largely enhanced by paramagnetic contrast agents, mainly $Gd^{3+}$ chelates or iron oxide nanoparticles [11]. In an advanced stage of AD, the iron content of the plaques allows their detection with specific MRI acquisition sequences without any contrast agent, leading to hypointense spots in $T_2$-, $T_2^*$-, or susceptibility-weighted images [12]. However, it requires high magnetic fields (7 T or more) and long acquisition times, which are impracticable in clinical MRI. The detection of plaques weakly loaded with iron requires the use of exogenous contrast agents. Contrast-agent-aided MRI studies reported to visualize AD plaques in transgenic mice include the use of ^{19}F-labeled compounds for ^{19}F MRI [13] and $Gd^{3+}$ complexes or ultrasmall superparamagnetic iron oxide conjugated with modified human $Aβ_{1–40}$ or human $Aβ_{1–42}$ peptide (e.g., with putrescine) able to cross the BBB [14–17] or ultrasmall superparamagnetic iron oxide conjugated with Aβ-specific peptides selected using the phage display technique [18]. Owing to the large size of these paramagnetic probes, several days (weeks) were necessary to label the amyloid plaques in the transgenic mouse brain in vivo, and

in most cases intra-carotid mannitol treatment was also used to enhance the BBB permeability of the agent.

Given the high electron spin and slow electronic relaxation of the $Gd^{3+}$ ion, $Gd^{3+}$ complexes are the most widely used MRI contrast materials, ensuring positive contrast [11]. The efficacy of a contrast agent is measured by its relaxivity, defined as the paramagnetic enhancement of the water proton relaxation rate normalized to 1 mM concentration of $Gd^{3+}$ [11, 19]. The inner-sphere relaxivity term is determined by the microscopic parameters of the $Gd^{3+}$ complex, the most important being the hydration number ($q$), the rotational correlation time ($\tau_R$), the water exchange rate ($k_{ex}$), and the electron spin relaxation times ($T_{1e}$, $T_{2e}$) [19]. The values of $\tau_R$ and $k_{ex}$ of the $Gd^{3+}$ complexes can be tuned by appropriate ligand design in order to optimize relaxivity. The maximum relaxivities predicted by the Solomon–Bloembergen–Morgan (SBM) theory can only be attained by chelates displaying simultaneous optimization of $k_{ex}$ and $\tau_R$ [11].

Imaging probes with multimodal features (e.g., MRI/PET, MRI/SPECT, or MRI/optical imaging) would be particularly useful for the diagnosis of AD. The most straightforward design is based on metal chelating agents that can accommodate different metal ions with capabilities in various imaging modalities, conjugated to specific amyloid-targeting units. Metal complexes could offer significant advantages, including longer half-lives of available metal-based PET/SPECT tracers and optimal spatial resolution when MRI is concerned. Recently, in a preliminary communication we have reported the ligand $L_1$ to create potential metal-based multimodal imaging probes for the detection of amyloid plaques in AD [20] (Fig. 1). We have conjugated an optimized derivative of PiB, a well-established marker of Aβ plaques, to 1,4,7,10-tetra-azacyclododecane-1,4,7-triacetic acid (DO3A) monoamide, which is capable of forming stable, noncharged complexes with different trivalent metal ions, including $Gd^{3+}$ for MRI applications, $^{111}In^{3+}$ for SPECT applications, and $^{68}Ga^{3+}$ for PET applications. In addition, the PiB unit is fluorescent, and can be traced with optical microscopy, representing another possible detection mode of the agent. The ligand $L_1$ coordinated to $Gd^{3+}$ showed interesting relaxivity, which further increased on binding to the amyloid peptide. Ex vivo immunohistochemical studies showed that the complexes selectively target Aβ plaques on AD human brain tissue. Ex vivo biodistribution data obtained with the $^{111}In$ analogue pointed to a moderate BBB penetration in adult male Swiss mice (without amyloid deposits), with 0.36 % of the injected dose per gram of tissue in the cortex at 2 min after injection.

We report the synthesis of two novel DO3A monoamide derivative ligands conjugated to the PiB moiety, $L_2$ and $L_3$, that possess linkers of differing length and chemical

**Fig. 1** Structure of the Gd(L$_x$)
($x = 1, 2, 3$) complexes
investigated



**GdL$_1$**          **GdL$_2$**          **GdL$_3$**
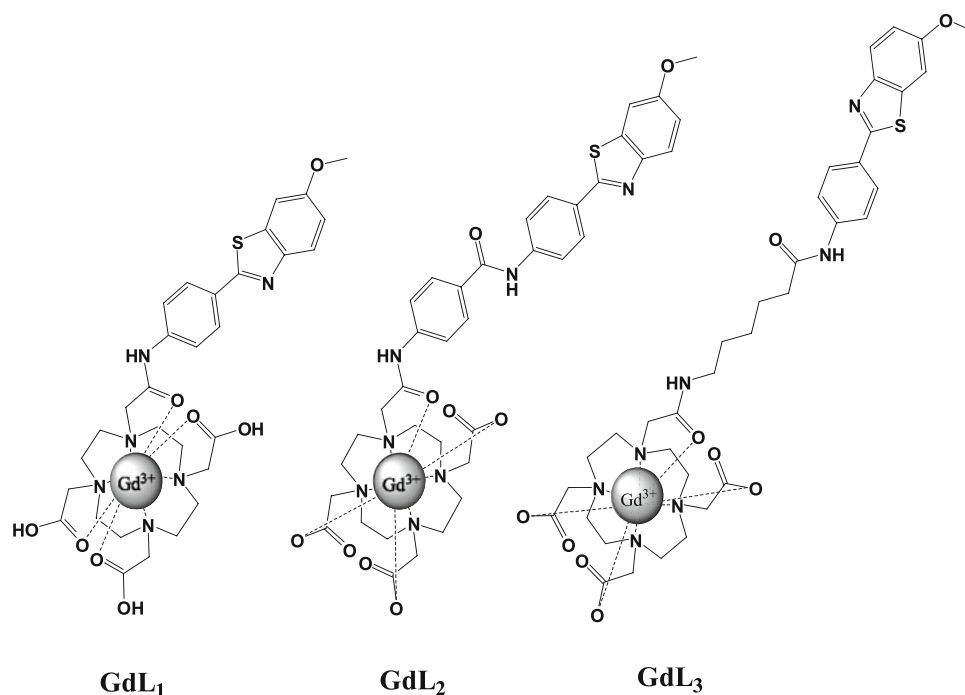
structure between the macrocycle and the amyloid-targeting moiety (Fig. 1). L$_2$ contains an extra 4-acetamidobenzamide group in the linker and L$_3$ has a longer aliphatic 6-acetamidohexanamide spacer. With the introduction of these different linkers, the hydrophobic properties and flexibility of the ligand can be modulated in order to optimize the target binding properties, the BBB permeation, and the relaxivity of the Gd$^{3+}$-based probe. Besides a gadolinium(III) diethylenetriaminepentaacetic acid (DTPA)–curcumin conjugate reported recently [21], these are the first low molecular weight, potential MRI contrast agents bearing a specific unit that allows targeting of amyloid plaques. We describe the characterization of the most relevant physicochemical parameters for the use of these complexes as MRI probes for Aβ detection. These studies include the assessment of (1) the octanol–water partition coefficients, which characterize the lipophilicity of the complexes, (2) micelle formation in aqueous solution, (3) the parameters influencing relaxivity via a combined $^{17}$O NMR and $^1$H nuclear magnetic relaxation dispersion (NMRD) study, and (4) the binding of the complexes to Aβ$_{1-40}$ peptide and to human serum albumin (HSA).

## Materials and methods

### Reagents and solutions

Chemicals were purchased from Sigma-Aldrich, Alfa Aesar, and CheMatech (DO3A-*t*-Bu$_3$) and were used

without further purification. Analytical grade solvents were used and were not purified further unless specified.

Reactions were monitored by thin-layer chromatography (TLC) on Kieselgel 60 F254 (Merck) on an aluminum support, with detection by examination under UV light (254 nm), by adsorption of iodine vapor, by spraying with ninhydrin, and by coloration of the complex with Dragendorff solutions. Polar affinity chromatography was performed with silica gel (Sigma-Aldrich). $^1$H and $^{13}$C NMR spectra were recorded with a Bruker Avance-500 (11.7-T) spectrometer operating at 500.132 and 125.769 MHz for $^1$H and $^{13}$C, respectively. Chemical shifts ($\delta$) are given in parts per million relative to CDCl$_3$ solvent ($^1$H, $\delta$ 7.27; $^{13}$C, $\delta$ 77.36) as an internal reference. For $^1$H and $^{13}$C NMR spectra recorded in D$_2$O, chemical shifts are given in parts per million relative to trimethylsilylpropionic acid as an internal reference ($^1$H, $\delta$ 0.0) and *tert*-butanol as an external reference ($^{13}$C, CH$_3$ $\delta$ 30.29). Mass spectrometry was performed at the Centre de Biophysique Moléculaire du CNRS in Orléans, France.
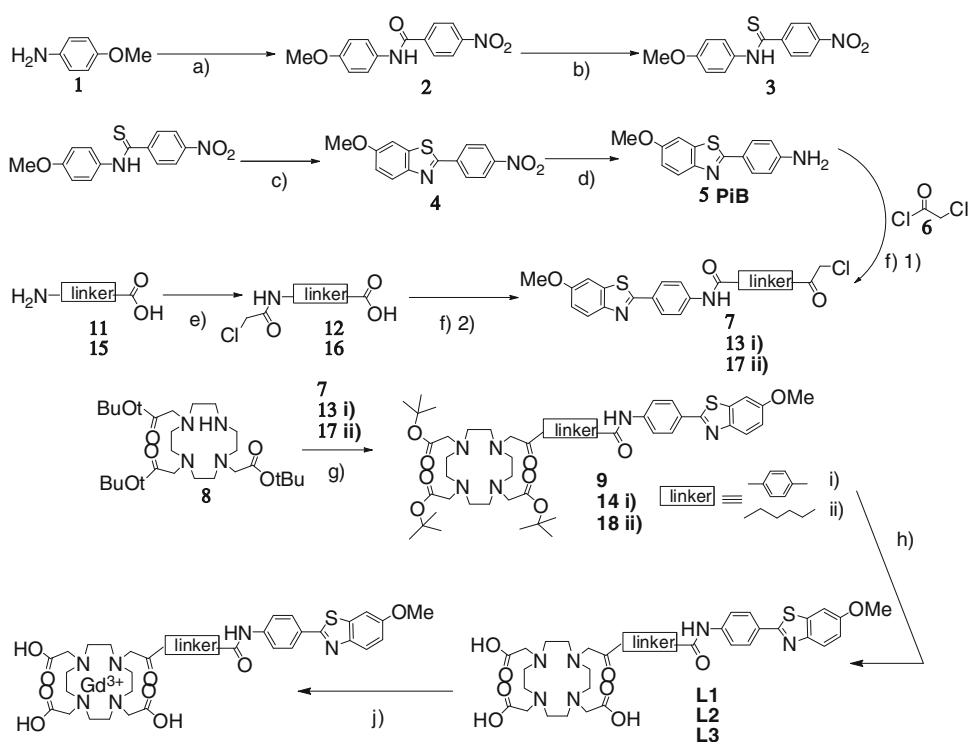
### Synthesis

Gd(L$_1$), Gd(L$_2$), and Gd(L$_3$) were synthesized according to Scheme 1. The synthesis of the common intermediates **2–5** and of Gd(L$_1$) was previously reported [20]. The chemical structures and atom numbering schemes for the synthesized compounds are shown in Figs. S1–S7.

**Scheme 1** Synthesis of Gd(L$_x$). The reagents and conditions were as follows: *a* tetrahydrofuran, NEt$_3$, 4-nitrobenzoyl chloride, 273 K, 96 %; *b* chlorobenzene, Lawesson's reagent, reflux, 85 %; *c* 10 % NaOH, K$_3$Fe(CN)$_6$, reflux, 53 %; *d* SnCl$_2$, EtOH, reflux, 92 %; *e* ClCH$_2$COCl (**6**), CH$_2$Cl$_2$, NaOH$_{aq}$, room temperature, 72–86 %; *f 1* Pittsburgh compound B (*PiB*) (**5**), K$_2$CO$_3$, CH$_3$CN or (CH$_3$)$_2$CO, room temperature, 50–82 %; *f 2* SOCl$_2$, Cl$_3$CH, reflux; *g* DO3A-*t*-Bu$_3$ (**8**), K$_2$CO$_3$, CH$_3$CN, room temperature, 38–93 %; *h* CH$_2$Cl$_2$, trifluoroacetic acid, 318 K, 73–79 %; *j* GdCl$_3$, pH 7



## Synthesis of L$_2$

### 4-(2-Chloroacetamido)benzoic acid

A biphasic reaction of **11** (1.2 g, 8.8 mmol) in 45 mL of CH$_2$Cl$_2$ and an aqueous 0.1 M NaOH solution was performed by adding a solution of chloroacetyl chloride (**6**) (0.9 mL, 11.2 mmol) in 15 mL of CH$_2$Cl$_2$. The mixture was stirred at room temperature for 3 h and the aqueous phase was acidified to pH $\sim$2 with an aqueous solution of 0.2 M HCl. The solution was extracted with CH$_2$Cl$_2$ (6 × 15 mL). The organic phase was washed with 10 mL of water, dried over MgSO$_4$, and the solvent was evaporated. The crude product was dissolved in a small amount of acetone, diethyl ether was added afterwards, and the solution was stored at 268 K overnight. White crystals were filtered to give 1.56 g of 4-(2-chloroacetamido)benzoic acid (**12**) (82 %) (Fig. S8). $^1$H NMR (CDCl$_3$, 298 K, 500 MHz): $\delta$ (ppm) 4.29 (s, 2H, H-9), 7.71 (d, $J = 8.5$ Hz, 2H, H-4, H-6), 7.91 (d, $J = 8.5$ Hz, 2H, H-3, H-7), 10.66 (s, –OH). $^{13}$C NMR (CDCl$_3$, 298 K, 126 MHz): $\delta$ (ppm) 44.0 (C-9), 119.0 (C-4, C-6), 130.8 (C-3, C-7), 142.9 (C-2), 165.5 (C-8), 167.3 (C-1).

### 4-(2-Chloroacetamido)-N-(4-(6-methoxybenzo[d]thiazol-2-yl)phenyl)benzamide

A solution of **12** (1.2 g, 5.6 mmol) was solubilized in SOCl$_2$ for 2 h at 323 K. The SOCl$_2$ was evaporated under a vacuum, with heating at 313 K, and the crude product (1.2 g, 5.2 mmol) was added to a 45-mL acetone solution containing **5** (1.2 g, 4.7 mmol) with potassium carbonate (2.14 g, 15.6 mmol), and the mixture was stirred overnight. The solid was filtered off and washed with acetone, and then the solvents were evaporated. The product obtained was recrystallized in acetonitrile to give 1.05 g of 4-(2-chloro acetamido)-N-(4-(6-methoxybenzo[d]thiazol-2-yl)phenyl) benzamide (**13**) (50 %) (Fig. S9). $^1$H NMR (dimethyl sulfoxide, 298 K, 500 MHz): $\delta$ (ppm) 3.86 (s, 3H, H-23), 4.32 (s, 2H, H-1), 7.123 (d, $J = 8.6$ Hz, 1H, H-20), 7.7–8.13 (m, 10H, H-18, H-21, H-5, H-4, H-7, H-8, H-12, H-11, H-14, H-15), 10.44 (s, NH), 10.62 (s, NH). $^{13}$C NMR (dimethyl sulfoxide, 298 K, 126 MHz): $\delta$ (ppm) 43.6 (C-1), 55.8 (C-23), 104.9 (C-18), 118.6 (C-11, C-15), 119.1 (C-20), 120.4 (C-4, C-8), 123.2 (C-21), 127.5 (C-12, C-14), 128.1 (C-13), 128.9 (C-5, C-7), 129.6 (C-6), 131.9 (C-17), 135.8 (C-10), 141.6 (C-3), 141.8 (C-22), 148.1 (C-19), 157.4 (C-9), 164.4 (C-2), 165.1 (C-16).

### Tri-tert-butyl-2,2′,2″-(10-(2-((4-(6-methoxybenzo[d] thiazol-2-yl)phenyl)carbamoyl)phenyl)amino)-2-oxoethyl)-1,4,7,10-tetraazacyclododecane-1,4,7-triyl)triacetate

To a solution of DO3A-*t*-Bu$_3$ (**8**) (300 mg, 0.58 mmol) and potassium carbonate (226 mg, 2 mmol) in 20 mL of dry acetonitrile was added a solution of *13* (316 mg, 0.7 mmol) in 15 mL of dry acetonitrile at room temperature. The reaction mixture was stirred for 48 h at room temperature

and the reaction was followed by TLC. The solid was filtered off and the solvent was evaporated. The crude product was purified by flash chromatography with dichloromethane–ethyl acetate (9:2). Tri-*tert*-butyl-2,2′,2″-(10-(2-((4-(6-methoxybenzo[*d*]thiazol-2-yl)phenyl)carbamoyl) phenyl)amino)-2-oxoethyl)-1,4,7,10-tetraazacyclododecane-1,4,7-triyl)triacetate (**14**) (200 mg) was obtained as an orange oil (38 %) (Fig. S10). $^1$H NMR (CDCl$_3$, 298 K, 500 MHz): $\delta$ (ppm) 1.42 (bs, 27H, –O*t*-Bu, H-34, H-35), 2.80–3.44 (m, 22H, H-25, H-24, H-26, H-27, H-23, H-28, H-29), 3.84 (s, 3H, H-7), 7.02–8.07 (m, 11H, H-1, H-5, H-4, H-10, H-14, H-11, H-13, H-21, H-17, H-20, H-18), 10.16 (s, NH), 11.19 (s, NH). $^{13}$C NMR (CDCl$_3$, 298 K, 126 MHz): $\delta$ (ppm) 27.9 (C-34, C-35), 42.3 (C-24, C-25, C-26, C-27), 45.4 (C-29, C-28), 67.3 (C-23), 82.0 (C-32), 82.1 (C-33), 104.1 (C-1), 115.4 (C-5), 119.4 (C-11, C-13), 120.8 (C-20, C-18), 123.3 (C-4), 124.7 (C-12), 127.7 (C-10, C-14), 128.4 (C-16), 128.8 (C-21, C-17), 130.9 (C-2), 136.3 (C-9), 141.7 (C-19), 142.4 (C-3), 148.7 (C-6), 157.5 (C-8), 164.6 (C-15), 165.5 (C-22), 166.1 (C-30), 171.4 (C-31).

### 2,2′,2″(10-(2-((4-(6-Methoxybenzo[d]thiazol-2-yl)phenyl)carbamoyl)phenyl)amino)-2-oxoethyl)-1,4,7,10-tetraazacyclododecane-1,4,7-triyl)triacetic acid (L$_2$)

Compound **14** (200 mg, 0.22 mmol) was dissolved in a mixture of trifluoroacetic acid and dry dichloromethane (1:1) and the resulting mixture was heated at 318 K overnight. The solvents were evaporated and the crude product was dried under a vacuum. The crude product was dissolved in a small amount of absolute ethanol and then diethyl ether was added. The mixture was allowed to stand overnight at 268 K. The yellowish precipitate (130 mg) was filtered off and dried under a vacuum (78 %) (Fig. S11). $^1$H NMR (D$_2$O, 323 K, 500 MHz): $\delta$ (ppm) 3.60–4.13 (bs, 24H, H-23, H-28, H-29, H-25, H-24, H-26, H-27), 4.44 (s, 3H, H-7), 6.87–7.92 (m, 11H, H-1, H-4, H-5, H-10, H-14, H-11, H-13, H-21, H-17, H-20, H-18). High-resolution mass spectrometry (electrospray ionization): *m/z*: calcd for C$_{37}$H$_{43}$N$_7$O$_9$S 761.284, found 761.244.

### Synthesis of L$_3$

### 6-(2-Chloroacetamido)hexanoic acid

To a biphasic mixture containing 15 (1.5 g, 11.4 mmol) in 45 mL of CH$_2$Cl$_2$ and an aqueous solution of 0.1 M NaOH, a solution of **6** (1.05 mL, 13.08 mmol) in 15 mL of CH$_2$Cl$_2$ was added. The mixture was stirred 3 h at room temperature and the aqueous phase was acidified to pH ~2 with an aqueous solution of 0.2 M HCl. The solution was extracted with CH$_2$Cl$_2$ (6 × 15 mL). The organic phase was washed with 10 mL of water, dried over MgSO$_4$, and the solvent was evaporated. The crude product was dissolved in a small amount of acetone and diethyl ether was added afterwards, and the solution was stored at 268 K overnight. White crystals were filtered off to give 1.7 g of 6-(2-chloroacetamido)hexanoic acid (**16**) (72 %) (Fig. S12). $^1$H NMR (CDCl$_3$, 298 K, 500 MHz): $\delta$ (ppm) 1.39 (m, 2H, H-4), 1.57 (m, 2H, H-5), 1.65 (m, 2H, H-3), 2.35 (t, 2H, H-2), 3.31 (m, 2H, H-6), 6.67 (s, 1H, –NH).

### 6-(2-Chloroacetamido)-N-(4-(6-methoxybenzo[d]thiazol-2-yl)phenyl)hexanamide

A solution of **16** (1.2 g, 5.6 mmol) was solubilized in SOCl$_2$ for 1 h at 298 K. The SOCl$_2$ was evaporated under a vacuum at 298 K, solubilized in chloroform, and extracted with a solution of aqueous NaOH (pH ~9). The crude chlorinated product (1.2 g, 5.2 mmol) was added to a 45-mL acetonitrile solution containing **5** (1.2 g, 4.7 mmol) with potassium carbonate (2.14 g, 15.6 mmol) and the mixture was stirred overnight at room temperature. The solid was filtered off and washed with acetonitrile, and then the solvents were evaporated. The product obtained was recrystallized in acetonitrile to give 2.04 g of 6-(2-chloroacetamido)-N-(4-(6-methoxybenzo[*d*]thiazol-2-yl)phenyl) hexanamide (**17**) (82 %) (Fig. S13). $^1$H NMR (CDCl$_3$, 298 K, 500 MHz): $\delta$ (ppm) 1.30 (m, 2H, H-18), 1.45 (m, 2H, H-19), 1.60 (m, 2H, H-17), 2.34 (t, 2H, H-16), 3.10 (m, 2H, H-20), 3.85 (s, 3H, –OCH$_3$, H-7), 4.40 (s, 2H, H-22), 7.11 (bd, 1H, H-5), 7.68 (bs, 1H, H-1), 7.76 (bd, 2H, H-11, H-13), 7.89 (bd, 1H, H-4), 7.96 (bd, 2H, H-10, H-14), 8.20 (s, –NH), 10.18 (s, –NH).

### Tri-tert-butyl-2,2′,2″-(10-(2-((6-((4-(6-methoxybenzo[d]thiazol-2-yl)phenyl)amino)6-oxohexyl)amino)-2-oxoethyl)-1,4,7,10-tetraazacyclododecane-1,4,7-triyl)triacetate

To a solution of **8** (600 mg, 1.16 mmol) and potassium carbonate (552 mg, 4 mmol) in 20 mL of dry acetonitrile was added a solution of **17** (400 mg, 0.89 mmol) in 15 mL of dry acetonitrile. The reaction mixture was stirred for 48 h at room temperature and the reaction was followed by TLC. The solid was filtered off and the solvent was evaporated. The crude product was purified by flash chromatography with dichloromethane–ethyl acetate (9:4). Tri-tert-butyl-2,2′,2″-(10-(2-((6-((4-(6-methoxybenzo[*d*] thiazol-2-yl)phenyl)amino)6-oxohexyl)amino)-2-oxoethyl)-1,4,7,10-tetraazacyclododecane-1,4,7-triyl)triacetate (**18**) (750 mg) was obtained as a yellow oil (93 %) (Fig. S14). $^1$H NMR (CDCl$_3$, 298 K, 500 MHz): $\delta$ (ppm) 1.25 (t, 27H, –O*t*-Bu, H-33, H-34), 1.46 (bs, 2H, H-18), 1.60 (bs, 4H, H-19, H-17), 2.43 (bs, 2H, H-16), 2.67 (s, 16H, H-25, H-26, H-23, H-24), 2.74 (s, 8H, H-22, H-27, H-28), 3.06 (bs, 2H, H-20), 3.7 (s, 3H, –OCH$_3$, H-7), 6.84 (bd, *J* = 8.8 Hz, 1H,

H-5), 7.10 (bs, 1H, H-1), 7.67 (d, $J = 8.8$ Hz, 1H, H-4), 7.77 (d, $J = 8.3$ Hz, 2H, H-11, H-13), 7.89 (d, $J = 8.3$ Hz, 2H, H-14, H-10), 8.26 (s, NH), 10.18 (s, NH). $^{13}$C NMR (CDCl$_3$, 298 K, 126 MHz): $\delta$ (ppm) 25.0 (C-18), 25.6 (C-17), 27.8 (C-34), 27.9 (C-33), 27.9 (C-22), 28.1 (C-19), 37.1 (C-16), 38.4 (C-20), 55.4 (C-25, C-26), 55.6 (C-27, C-28), 55.8 (C-24, C-23), 56.2 (C-7), 81.7 (C-32), 81.8 (C-31), 104.2 (C-1), 115.3 (C-5), 112.0 (C-11, C-13), 123.2 (C-4), 127.5 (C-10, C-14), 128.0 (C-9), 136.1 (C-2), 142.4 (C-12), 148.7 (C-3), 157.5 (C-6), 165.7 (C-21), 171.6 (C-8), 172.3 (C-29, C-30), 173.5 (C-15).

### 2,2′,2″-(10-(2-((6-((4-(6-Methoxybenzo[d]thiazol-2-yl)phenyl)amino)-6-oxohexyl)amino)-2-oxoethyl)-1,4,7,10-tetraazacyclododecane-1,4,7-triyl)triacetic acid (L$_3$)

Compound **18** (750 mg, 0.81 mmol) was dissolved in a mixture of trifluoroacetic acid and dry dichloromethane (1:1) and the resulting mixture was heated at 318 K overnight. The solvents were evaporated and the crude product was dried under a vacuum. The crude product was dissolved in a small amount of CH$_2$Cl$_2$, and then acetone was added to the mixture and the resulting mixture was left overnight at 268 K for recrystallization. Yellowish crystals (450 mg) were filtered off and dried under a vacuum (73 %) (Fig. S15). $^1$H NMR (D$_2$O, 323 K, 500 MHz): $\delta$ (ppm) 1.72 (bs, 2H, H-18), 1.91 (bs, 2H, H-19), 1.98 (bs, 2H, H-17), 2.67 (s, 2H, H-20), 3.6 (bs, 12H, H-25, H-26, H-16), 3.70 (bs, 4H, H-24), 3.89 (bs, 3H, H-7), 4.10 (bs, 4H, H-27), 4.26 (bs, 2H, H-28), 4.31 (bs, 2H, H-22), 6.98 (bs, 1H, H-5), 7.17 (bs, 1H, H-1), 7.59 (bs, 4H, H-10, H-14, H-11, H-13), 7.87 (bs, 1H, H-4). $^{13}$C NMR (D$_2$O, 323 K, 126 MHz): $\delta$ (ppm) 25.4 (C-17), 26.6 (C-18), 28.8 (C-19), 37.3 (C-16), 40.1 (C-20), 49.9 (C-23, C-24), 51.3 (C-25, C-26), 54.5 (C-28), 55.4 (C-22), 55.9 (–O–CH$_3$, C-7), 56.2 (C-27), 104.8 (C-1), 116.5 (C-5), 120.6 (C-11,13), 122.6 (C-4), 127.3 (C-9), 128.0 (C-10,14), 135.3 (C-2), 141.2 (C-12), 146.3 (C-3), 157.9 (C-6), 163.0 (C-21), 163.3 (C-8), 166.5 (C-15), 172.6 (C-30), 174.8 (C-29). High-resolution mass spectrometry (electrospray ionization): $m/z$: calcd for C$_{36}$H$_{49}$N$_7$O$_9$S 755.331, found 755.265.

### Sample preparation

Gd(L$_x$) ($x = 1, 2, 3$) complexes were prepared by mixing solutions of GdCl$_3$ and the ligand L$_x$ in equimolar quantities and adjusting the pH to 7 with aqueous NaOH (0.1 mM). The solutions were allowed to react for 24 h at 333 K while the pH was regularly controlled. The absence of free metal ion was checked in each sample by using the xylenol orange test [22]. In the relaxometric HSA binding studies, 0.6 mM HSA (4 %) solutions were used. For the Aβ$_{1–40}$ binding studies, the peptide was added directly from the bottle to an equimolar solution of Gd(L$_x$) (200 μM) in 0.05 M $N$-(2-hydroxyethyl)piperazine-$N'$-ethanesulfonic acid buffer at pH 7 and the sample was sonicated. Milli-Q water was always used to avoid metal contamination. The sample containing the reconstituted peptide was used immediately to avoid degradation in solution.

### Determination of the octanol–water partition coefficient

The partition coefficient was determined as the ratio of the concentration of the compound in octanol and concentration of the compound in the aqueous phase (Eq. 1):

$$\text{Partition coefficient } (P) = \frac{[\text{solute}] \text{ octanol phase}}{[\text{solute}] \text{ aqueous phase}}. \quad (1)$$

The logarithm of the partition coefficient is referred to as the log $P$ value.

The "shake flask" method was used for the determination of log $P$ [23]. Water saturated with octanol and octanol saturated with water were used in the experiments. The benzothiazol ring absorbs strongly at approximately 330 nm; therefore, the partition was quantified using UV spectrophotometry with a PerkinElmer Lambda 19 UV–vis spectrophotometer [24]. For each phase, the maximum wavelength was verified. A 1:1 volume ratio was used for the partitioning of the solution with Gd(L$_x$). In a 2-mL Eppendorf tube, 0.5 mL of a 100 μM solution of Gd(L$_x$) was added to 0.5 mL of the saturated phase of 1-octanol. Each sample was centrifuged for 30 min. Gd(L$_x$) concentrations were determined in each phase using standard curves.

### $^1$H NMRD measurements

$^1$H NMRD profiles were recorded with a Stelar SMARtracer fast field cycling NMR relaxometer (0.01–10 MHz) and a Bruker WP80 NMR electromagnet (20, 40, 60, and 80 MHz) adapted to variable-field measurements and controlled by a SMARtracer PC-NMR console. The temperature was monitored by a VTC91 temperature control unit and was maintained by a gas flow. The temperature was determined by previous calibration with a platinum resistance temperature probe. The longitudinal relaxation rates ($1/T_1$) were determined in water. Measurements were performed at 298 and 310 K.

### $^{17}$O NMR experiments

Variable-temperature $^{17}$O NMR measurements were performed with a Bruker Avance-500 (11.7-T) spectrometer, and a BVT-3000 temperature control unit was used to stabilize the temperature. The temperature was calculated according to a previous calibration with ethylene glycol

and methanol [25]. The samples were sealed in glass spheres that fitted into 10 mm outer diameter NMR tubes, to eliminate susceptibility corrections to the chemical shifts [19, 26]. Longitudinal relaxation rates ($1/T_1$) were obtained by the inversion recovery method and transverse relaxation rates ($1/T_2$) were obtained by the Carr–Purcell–Meiboom–Gill spin-echo technique. Acidified water of pH 3.4 was used as an external reference. $^{17}O$-enriched water (10 % $H_2^{17}O$, CortectNet) was added to the solutions to reach around 1 % enrichment.

### Determination of the affinity constants for HSA binding of $Gd(L_1)$ and $Gd(L_3)$

Affinity constants with regard to HSA (defatted, from Sigma-Aldrich, 0.01 % or less fatty acids and 1 % or less globulins) were assessed by proton relaxation enhancement (PRE) measurements. The proton relaxation rates at increasing concentrations of the protein or the metal chelate were measured using a Bruker WP80 NMR electromagnet adapted to variable-field measurements and controlled by a SMARtracer PC-NMR console (40 MHz, 310 K). For the E-titration [the concentration of $Gd(L_1)$ or $Gd(L_3)$ is constant, and the protein concentration is varied], the $Gd(L_1)$ and $Gd(L_3)$ concentrations were 0.1 mM, and for the M-titration (the protein concentration is constant and the complex concentration is varied), the HSA concentration was 0.6 mM.

## Results and discussion

### Synthesis

The synthesis of the benzothiazole targeting moiety was done according to Mathis et al. [5, 27, 28]. The general strategy for the synthesis of the ligands is outlined in Scheme 1. We performed the amide formation by the acylation of 4-methoxyaniline (**1**) with 4-nitrobenzoyl chloride to form the product **2** in very high yield (96 %). Subsequently, compound **2** was made to react with half equivalents of Lawesson's reagent and the thiation occurred with a good yield, giving the corresponding thioamide **3**. The following reaction was the cyclization of compound **3** in the *ortho* position of the methoxyphenyl ring to form 6-methoxy-2-(4-nitrophenyl)benzo[*d*]thiazole (**4**) [29]. Compound **4** was reacted with stannous chloride to reduce the nitrophenyl group, to obtain, with a remarkably high yield, the envisaged benzothiazol derivative 4-(6-methoxybenzol[*d*]thiazol-2-yl)aniline (**5**), containing a free terminal primary amine function.

Acylation of compound **5** with chloroacetyl chloride (**6**) was performed in acetone. The available primary amine

from the aniline moiety undergoes a fast reaction with the chloroacyl group, forming product **7** with good yield after recrystallization. To obtain the intermediate **13**, the reagent 4-aminobenzoic acid (**11**) was reacted with **6** under Schotten–Baumann conditions [30, 31], giving the corresponding amide **12**. Compound **12** was then activated by chlorination with thionyl chloride ($SOCl_2$). Consequently, 4-(2-chloroacetamido)benzoyl chloride was introduced in a fast reaction with compound **5** using acetone as the solvent, to achieve the condensation and obtain the final intermediate 4-(2-chloroactetamido)-N-(4-(6-methoxybenzo[*d*]thiazol-2-yl)phenyl)benzamide (**13**).
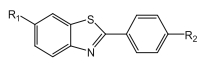
The preparation of the longer linker 6-acetoamidohexanamide required the acylation of compound **15**. The intermediate product 6-(2-chloroacetoamido)hexanoic acid (**16**) obtained was reacted with $SOCl_2$ to achieve the chlorination of the carboxylic acid in very mild conditions ($CH_2Cl_2$, 298 K) and to minimize side reactions (cyclization). The very reactive 2-chloro-6-acetoamidohexanamide chloride obtained before was reacted with compound **5** with the primary free amine available and made possible the condensation, giving 6-2-chloroactetamido)-N-(4-(6-methoxybenzo[*d*]thiazol-2-yl)phenyl)hexanamide (**17**) in high yield.

Ligands $L_1$, $L_2$, and $L_3$ were obtained by the monoalkylation of the functionalized compound **8** with compounds **7**, **13**, and **17**. The reaction proceeded in acetonitrile at room temperature for 48 h. The acid-sensitive *tert*-butyl protecting groups were then removed with trifluoroacetic acid and the ligands with the free carboxylic acid available to form $Ln^{3+}$ complexes were obtained with global yields over the two last steps of 70, 30, and 68 % for $L_1$, $L_2$, and $L_3$, respectively.

### Lipophilicity of the complexes as determined by the partition coefficient

A contrast agent designed to detect amyloid plaques in the brain should optimally pass the BBB. The BBB permeability of a compound is determined by different factors, including lipophilicity, often expressed by the water–octanol partition coefficient, log $P_{oct/water}$, molecular weight, and plasma pharmacokinetics [32]. A low molecular weight and an amphiphilic character of the molecule are known to favor BBB permeability. Typically, compounds with log $P_{oct/water} \sim 2$ have optimal BBB penetration. The log $P_{oct/water}$ values obtained for $Gd(L_2)$ and $Gd(L_3)$, 0.32 and 0.03, respectively, are considerably higher than the value obtained for $Gd(L_1)$, −0.15 [20], owing to the more hydrophobic nature of their linker (Table 1). As expected, all these values are lower than those of the highly lipophilic PiB molecule or other phenylbenzothiazole derivatives [5, 32, 33].

**Table 1** Molecular weight (*MW*) and lipophilicity (log $P_{\text{oct/water}}$) of phenylbenzothiazole derivatives

| | log $P_{\text{oct/water}}$ | MW | References |
|---|---|---|---|
| Thioflavin T | 0.57 | 319 | [5] |
| $R_1$ is $CH_3$, $R_2$ is $NH_2$ | 2.6 | 240 | [5, 27] |
| $R_1$ is $CH_3$, $R_2$ is $NHCH_3$ | 2.6 | 254 | [5] |
| $R_1$ is $OCH_3$, $R_2$ is $NH_2$ | 1.9 | 256 | [5] |
| $R_1$ is OH, $R_2$ is $NHCH_3$ (PiB) | 1.23 | 256 | [33] |
| $R_1$ is OH, $R_2$ is ReO-TEEDA | 1.21 | 602 | [33] |
| $R_1$ is $OCH_3$, $R_2$ is ReO-TEEDA | 2.52 | 616 | [33] |
| $^{99m}$TcO-BAT-Bp-1 | 0.68 | 559 | [10] |
| $^{99m}$TcO-BAT-Bp-2 | 1.35 | 573 | [10] |
| $^{99m}$TcO-BAT-Bp-3 | 2.09 | 587 | [10] |
| Gd(L$_1$) | −0.15 | 842 | [20] |
| Gd(L$_2$) | 0.32 | 918 | This work |
| Gd(L$_3$) | 0.03 | 912 | This work |

BAT-Bp-1, bis(aminoethanethiol)-benzofuranpyridyl-NH$_2$; BAT-Bp-2, bis(aminoethanethiol)-benzofuranpyridyl-NH(CH$_3$); BAT-Bp-3, bis(aminoethanethiol)-benzofuranpyridyl-N(CH$_3$)$_2$; PiB, Pittsburgh compound B; TEEDA, ethylthiol-diethylenetriamine

Some rhenium and technetium complexes proposed as nuclear imaging probes for AD detection have been reported to have relatively high, close-to-optimal log $P_{\text{oct/water}}$ values, and correspondingly, they had interesting BBB passage in vivo [10]. These complexes are, however, structurally very different from our Gd$^{3+}$ chelates. In fact, it is not possible to create stable lanthanide complexes that are sterically as compact as those of technetium or rhenium, since Ln$^{3+}$ cations are much larger than M(V) (M is Tc, Re) cations in the MO$^{3+}$ oxocations [34] and need considerably more chelating functions to form stable and inert complexes. Moreover, the chemical nature of lanthanide ions requires strongly ionic coordinating functions. These factors all contribute to an increased hydrophilic character of the chelates. The addition of bulky lipophilic groups could increase the overall lipophilicity of the complex, but this would also increase the molecular weight, which disfavors BBB permeability. Indeed, low molecular weight compounds cross the BBB more efficiently with rates that seem to correlate inversely with the square root of their molecular weight [35], at least for compounds with a molecular weight 600. The molecular weights of Gd(L$_1$), Gd(L$_2$), and Gd(L$_3$) are 842, 918, and 912, respectively, which are above the optimal values. However, peptide derivatives with a molecular weight over 1,000 were shown to cross the BBB by passive diffusion [36, 37].

## Determination of the critical micellar concentration by $^1$H relaxivity measurements

Given the amphiphilic character of the Gd(L$_x$) chelates, they form micellar aggregates in aqueous solution. We
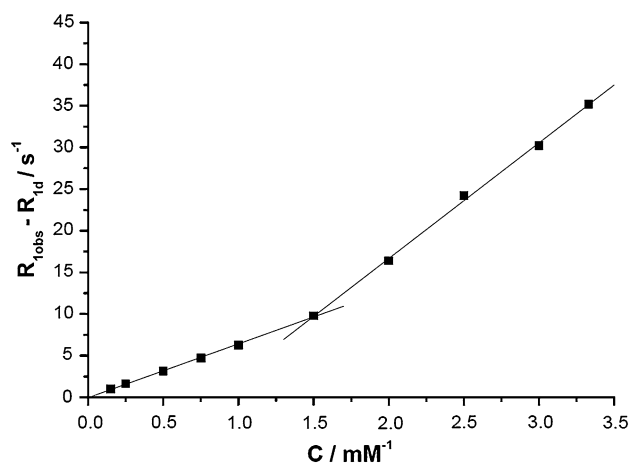


**Fig. 2** Paramagnetic contribution to the water $^1$H longitudinal relaxation rates as a function of the Gd(L$_3$) concentration at 40 MHz and 298 K

determined the critical micellar concentration (cmc) for the Gd(L$_3$) complex by relaxometric measurements [38]. The cmc for Gd(L$_1$) was reported previously [20]. The low solubility of Gd(L$_2$) (0.133 mM) does not allow assessment of the cmc. To obtain the cmc, the paramagnetic relaxation rates, $R_{1p}$, were plotted versus the Gd(L$_3$) concentration at 40 MHz, a magnetic field where the effect of slower rotation on relaxivity is the most pronounced and thus the relaxivity difference between the monomer and the aggregated state is important (Fig. 2).

At concentrations below the cmc no aggregates form, and under these conditions, only the monomeric chelate contributes to the paramagnetic $^1$H relaxation rate measured in solution, which is given by Eq. 2:

$$R_{1p} = R_1^{\text{obs}} - R_1^{\text{d}} = r_1^{\text{na}} \times C_{\text{Gd}} \qquad (2)$$

Here $R_d^1$ is the diamagnetic contribution to the longitudinal relaxation rate (the relaxation rate of pure water), $r_1^{\text{na}}$ represents the relaxivity of the free, nonaggregated Gd$^{3+}$ chelate (mM$^{-1}$ s$^{-1}$), and $C_{\text{Gd}}$ is the analytical Gd$^{3+}$ concentration.

At concentrations above the cmc, the measured relaxation rate is the sum of two contributions, one due to the chelate as a monomer (free surfactant) present at a concentration given by the cmc, and the other due to the aggregated form (micelles). The water $^1$H relaxation rate measured for the paramagnetic solution can be then expressed as in Eq. 3:

$$R_1^{\text{obs}} - R_1^{\text{d}} = (r_1^{\text{n.a}} - r_1^{\text{a}}) \times \text{cmc} + r_1^{\text{a}} \times C_{\text{Gd}} \qquad (3)$$

where $r_1^{\text{a}}$ is the relaxivity of the micellar (aggregated) form.

The cmc is determined from a plot of the paramagnetic relaxation rate versus the Gd$^{3+}$ concentration by a simultaneous least-squares fit of the two straight lines (Fig. 2). The slopes of these two lines define $r_1^{\text{na}}$ and $r_1^{\text{a}}$, below and

**Table 2** Relaxivities of the monomer ($r_1^{na}$) and the aggregated ($r_1^a$) form and critical micellar concentrations obtained from the $^1H$ relaxivity study for Gd(L$_x$) complexes (40 MHz, 298 K) compared with those for other micellar systems from the literature

| Complex | $r_1^{na}$ (mM$^{-1}$ s$^{-1}$) | $r_1^a$ (mM$^{-1}$ s$^{-1}$) | Critical micellar concentration (mM) |
|---|---|---|---|
| Gd(L$_1$)[a] | 6.4 | 13.9 | 1.49 |
| Gd(L$_3$)[b] | 6.1 ± 0.2 | 13.8 ± 0.4 | 1.00 ± 0.02 |
| Gd(DOTAC$_{10}$)$^{-}$[c,d] | 5.3 | 10.8 | 7.20 |
| Gd(DOTAC$_{12}$)$^{-}$[c,d] | 5.5 | 17.9 | 4.45 |
| Gd(DOTAC$_{14}$)$^{-}$[c,d] | 5.4 | 22.0 | 0.87 |
| Gd(DOTASAC$_{18}$)$^{-}$[c,d] | 10.5 | 17.0 | 0.06 |

See Fig. 1 for the structure of Gd(L$_1$), Gd(L$_2$), and Gd(L$_3$)

DOTAC$_{10}$, 1,4,7,10-tetraaza-1-(1-carboxymethylundecane)-4,7,10-triacetic acid cyclododecane; DOTAC$_{12}$, 1,4,7,10->tetraaza-1-(1-carboxymethyltridecane)-4,7,10-triacetic acid cyclododecane; DOTAC$_{14}$, 1,4,7,10-tetraaza-1-(1-carboxy-tert-butoxymethylquintodecane)-4,7,10-triacetic acid; DOTASAC$_{18}$, [2-(methyloctadecylamino)-2-oxoethyl]-1,4,7,10-tetraazacyclododecane-1,4,7,10-tetraacetic acid

[a] From [20]

[b] This work

[c] Parameters obtained at 60 MHz and 298 K

[d] From [38]

above the cmc, respectively. The values obtained for Gd(L$_3$) were $r_1^{na}$ = 6.1 mM$^{-1}$ s$^{-1}$ and $r_1^a$ = 13.8 mM$^{-1}$ s$^{-1}$ (298 K, 40 MHz), similar to those for Gd(L$_1$) (Table 2) [20]. The cmc for Gd(L$_3$) is 1.00 ± 0.02 mM, slightly lower than that for Gd(L$_1$) (Table 2), owing to the presence of the C6 lipophilic spacer chain. These values, when compared with those for previously studied hydrocarbon chain amphiphilic Gd$^{3+}$ complexes (Table 2) are similar to the cmc of complexes comprising relatively long, C$_{12}$–C$_{14}$ lipophilic tails, showing that the aromatic structures in Gd(L$_1$) and Gd(L$_3$) efficiently promote aggregation. The cmc has been previously determined at variable temperatures for other systems and it was found to be identical within the error at 298 and 310 K [38]. Therefore, we can consider that the cmc remains constant for our systems within this temperature range.

## $^{17}O$ NMR and $^1H$ NMRD measurements

NMRD profiles reflect the magnetic field dependency of the proton relaxivity ($r_1$) and are commonly used to characterize MRI contrast agents. $^1H$ NMRD profiles were recorded at 298 and 310 K over the frequency range 0.01–100 MHz for the Gd$^{3+}$ complexes at concentrations below and above the cmc, except for Gd(L$_2$), for which low solubility prevented working in the aggregated state. The NMRD curves recorded at low, 0.2 mM (L$_1$, L$_3$), or 0.1 mM (L$_2$) concentration are characteristic of low molecular weight complexes (Figs. 3a, b, S19). Even at these low concentrations, the

Gd(L$_x$) chelates exhibit approximately 50–60 % higher relaxivities than clinical contrast agents [39, 40]: $r_1$ = 6.30, 6.48, and 6.46 mM$^{-1}$ s$^{-1}$, respectively, for $x$ = 1, 2, and 3 (20 MHz, 298 K). These higher $r_1$ values are the consequence of a slower rotation, resulting from the presence of the bulky PiB moiety. When the concentration is increased to 5 mM, the NMRD profiles change considerably, and correspond to slowly tumbling systems with a typical high-field peak around 40 MHz (Fig. 3c, d). The features of the NMRD curve are influenced by the water exchange rate, electron relaxation parameters, and rotational correlation times. Therefore, NMRD measurements are usually combined with $^{17}O$ NMR measurements to assess all the parameters that determine proton relaxivity. By performing variable-temperature $^{17}O$ $T_2$ measurements, one can accurately determine the water exchange rate. The rotational correlation time can be assessed by performing variable-temperature $^{17}O$ $T_1$ measurements. On the other hand, variable-temperature measurements of the chemical shift difference between bulk and bound water ($\Delta\omega_r$), give an indication of the $q$ value. A reliable determination of the parameters common to $^1H$ NMRD and $^{17}O$ NMR is often performed through the simultaneous least-squares fitting of all the data obtained. Nevertheless, given the different concentrations typically used in NMRD and $^{17}O$ NMR measurements, such a simultaneous fit is not possible when concentration-dependent phenomena such as micellar aggregation occur in the system.

We performed a variable-temperature $^{17}O$ NMR study on an aqueous solution of Gd(L$_3$). The low water solubility of the other Gd$^{3+}$ complexes prevented $^{17}O$ NMR measurements, which require concentrations typically above 10 mM. Figure 4 shows the temperature dependency of the reduced $^{17}O$ chemical shifts ($\Delta\omega_r$), the transverse relaxation rates ($1/T_{2r}$), and the longitudinal relaxation rates ($1/T_{1r}$). For Gd(L$_3$), the transverse $^{17}O$ relaxation rates increase with decreasing temperatures above 320 K, indicating that this complex is in the fast exchange regime. At lower temperatures, the transverse relaxation rates correspond to a slow exchange regime. The reduced chemical shifts are in accordance with this trend.

In the slow exchange regime, the reduced transverse relaxation rates are directly determined by the water exchange rate. In the fast exchange regime, they are also influenced by the longitudinal electronic relaxation rate ($1/T_{1e}$) and the scalar coupling constant ($A/\hbar$). The reduced $^{17}O$ chemical shifts are determined by $A/\hbar$. Transverse $^{17}O$ relaxation is governed by the scalar relaxation mechanism, and thus contains no information on the rotational motion of the system. In contrast to $1/T_{2r}$, the longitudinal $^{17}O$ relaxation rates ($1/T_{1r}$) are determined by dipole–dipole and quadrupolar relaxation mechanisms, both related to rotation.
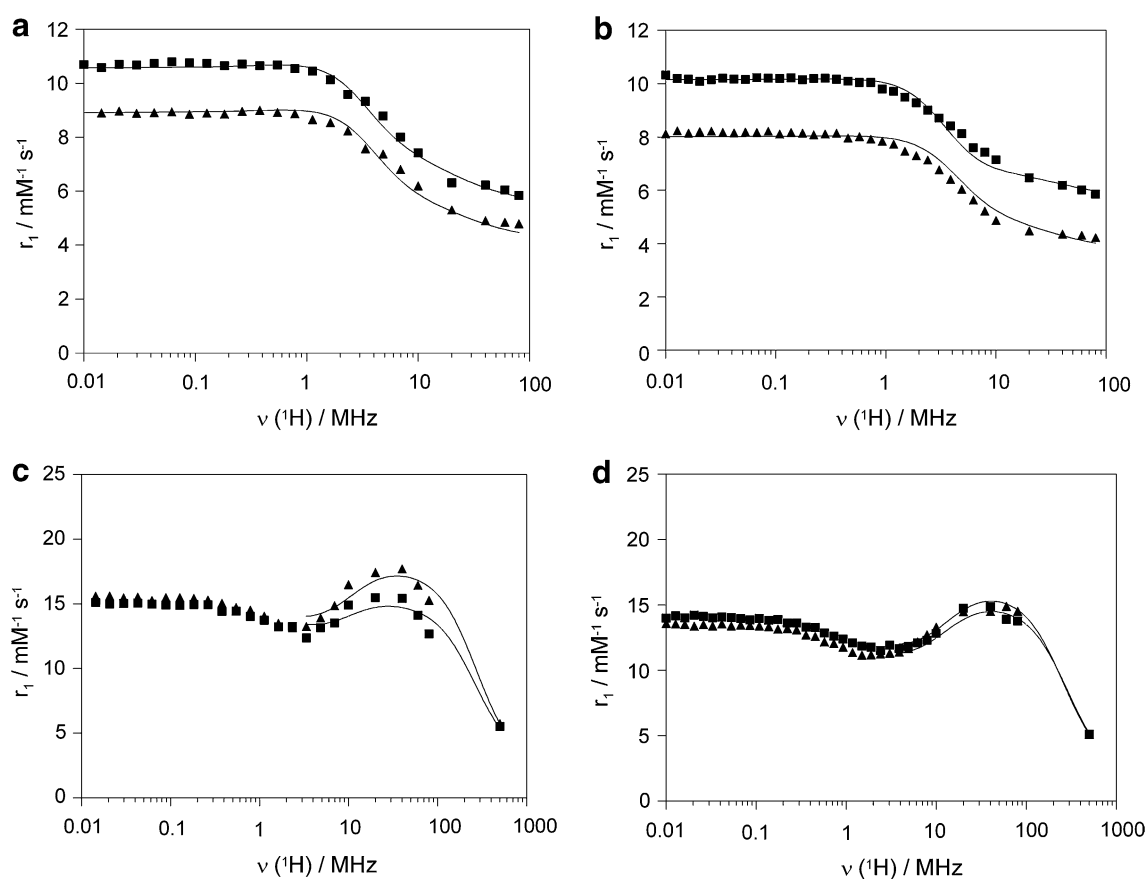
**Fig. 3** $^1$H nuclear magnetic relaxation dispersion (NMRD) profiles at 298 K (*squares*) and 310 K (*triangles*) of **a** Gd(L$_1$) at 0.2 mM concentration (momomer form), **b** Gd(L$_3$) at 0.2 mM concentration (momomer form), **c** Gd(L$_1$) at 5.0 mM concentration (micellar form), and **d** Gd(L$_3$) at 5.0 mM concentration (micellar form). The *solid lines* correspond to the fits as explained in the text

Since the $^{17}$O NMR and the NMRD data were obtained at different concentrations where the aggregation state of the Gd(L$_3$) complex is different, they were analyzed separately using the traditional SBM theory [11, 19]. Monohydration was assumed for all complexes—Gd(L$_x$) stands for [Gd(L$_x$)(H$_2$O)] throughout the text. For Gd(L$_3$), partially in the slow water exchange regime, the reduced $^{17}$O chemical shifts, and consequently the scalar coupling constant calculated, give direct indication of the hydration state and they clearly evidence one inner-sphere water molecule. For the NMRD data, we evaluated the curves both below and above the cmc (Figs. 3, S19). The theoretical equations and the details of the analysis are shown in the electronic supplementary material and the parameters obtained are given in Tables 3 and 4.

Above the cmc, the proton relaxation rates measured represent the sum of the contributions of the monomer complex, which is present at a concentration equal to the cmc, and of the aggregated state. Therefore, to calculate the relaxivity of the aggregated form, we subtracted the relaxivity contribution of the monomer from the relaxation rates measured above the cmc. The relaxivities calculated

in this way for the micellar form were fitted to the SBM theory by including the Lipari–Szabo treatment for the description of the rotational motion. In this approach, two kinds of motion are assumed to modulate the interaction causing the relaxation, namely a rapid, local motion which lies in the extreme narrowing limit and a slower, global motion. We calculated, therefore, $\tau_g$, the correlation time for the global motion (common to the whole micelle), and $\tau_l$, the correlation time for the fast local motion, which is specific for the individual relaxation axis, and is thus related to the motion of the individual Gd$^{3+}$ chelate units. The generalized order parameter, $S^2$, is a model-independent measure of the degree of spatial restriction of the local motion, with $S^2 = 0$ if the internal motion is isotropic and $S^2 = 1$ if the motion is completely restricted. In the fit of the micellar form, we used only the relaxivities above 4 MHz, where the validity of the SBM theory for slowly rotating systems is respected. The water exchange rate and the water exchange enthalpy were fixed for Gd(L$_3$) to the values obtained in the $^{17}$O NMR study (Table 3, Fig. 4). The Gd(L$_1$) complex in its micellar form exhibits a distinct and unusual temperature dependency: the relaxivities at
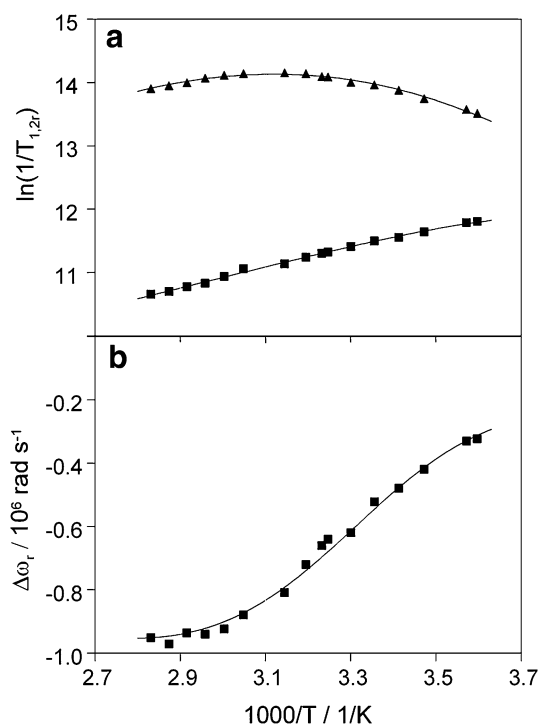
**Fig. 4** Temperature dependence of the reduced longitudinal (*a*, *squares*) and transverse (*a*, *triangles*) $^{17}$O relaxation rates and reduced chemical shifts (*b*) of Gd(L$_3$) in aqueous solution (*B* = 11.7 T, *c* = 10.28 mM)

**Table 3** Best-fit parameters obtained for [Gd(L$_3$)(H$_2$O)] from the analysis of $^{17}$O NMR data

| Parameters | [Gd(L$_3$)(H$_2$O)] | [Gd(DOTA)(H$_2$O)]$^-$ [39] |
|---|---|---|
| $k_{ex}^{298}$ ($10^6$ s$^{-1}$) | 2.8 ± 0.4 | 4.1 |
| $\Delta H^{\ddagger}$ (kJ mol$^{-1}$) | 32.0 ± 1.0 | 49.8 |
| $\Delta S^{\ddagger}$ (J mol$^{-1}$ K$^{-1}$) | 14 ± 4 | 48.5 |
| $E_R$ (kJ mol$^{-1}$) | 14.2 ± 0.2 | 16.1 |
| $\tau_{RO}^{298}$ (ps) | 601 ± 10 | 77 |
| $E_V$ (kJ mol$^{-1}$) | *1.0* | *1.0* |
| $\tau_V^{298}$ (ps) | 8.4 ± 1 | 11 |
| $\Delta^2$ ($10^{20}$ s$^{-2}$) | 0.28 ± 0.01 | 0.16 |
| $A/\hbar$ (MHz) | −3.7 ± 0.2 | −3.7 |

Values in *italics* were fixed in the fitting

DOTA, 1,4,7,10-tetraazacyclododecane-1,4,7,10-tetraacetic acid

**Table 4** Best-fit parameters obtained for the monomer forms of [Gd(L$_1$)(H$_2$O)], [Gd(L$_2$)(H$_2$O)], and [Gd(L$_3$)(H$_2$O)] from the analysis of NMR dispersion (NMRD) data below the critical micellar concentration

| Parameters | [Gd(L$_1$)(H$_2$O)] | [Gd(L$_2$)(H$_2$O)] | [Gd(L$_3$)(H$_2$O)] |
|---|---|---|---|
| $k_{ex}^{298}$ ($10^6$ s$^{-1}$) | *2.8* | *2.8* | *2.8* |
| $\Delta H^{\ddagger}$ (kJ mol$^{-1}$) | *32.0* | *32.0* | *32.0* |
| $E_R$ (kJ mol$^{-1}$) | 18.2 ± 0.2 | 37.2 ± 0.2 | 32.3 ± 0.8 |
| $\tau_{RH}^{298}$ (ps) | 130 ± 10 | 150 ± 10 | 141 ± 11 |
| $E_V$ (kJ mol$^{-1}$) | *1.0* | *1.0* | *1.0* |
| $\tau_V^{298}$ (ps) | 50 ± 5 | 27 ± 3 | 25 ± 3 |
| $\Delta^2$ ($10^{20}$ s$^{-2}$) | 0.11 ± 0.01 | 0.40 ± 0.01 | 0.26 ± 0.02 |

Values in *italics* were fixed in the fitting

**Table 5** Best-fit parameters obtained for the micellar forms of [Gd(L$_1$)(H$_2$O)] and [Gd(L$_3$)(H$_2$O)] from the analysis of NMRD data above the critical micellar concentration, after subtraction of the monomer relaxivities

| Parameters | [Gd(L$_1$)(H$_2$O)] | [Gd(L$_3$)(H$_2$O)] |
|---|---|---|
| $k_{ex}^{298}$ [$10^6$ s$^{-1}$] | 1.0 ± 0.1 | 2.8 |
| $\Delta H^{\ddagger}$ (kJ mol$^{-1}$) | 30.0 ± 0.2 | *32.0* |
| $E_l$ (kJ mol$^{-1}$) | 16 ± 0.2 | 16 ± 0.2 |
| $\tau_{lH}^{298}$ (ps) | 105 ± 10 | 102 ± 10 |
| $E_g$ (kJ mol$^{-1}$) | 16 ± 0.2 | 16 ± 0.2 |
| $\tau_{gH}^{298}$ (ns) | 12.0 ± 0.8 | 8.0 ± 0.5 |
| $S^2$ | 0.12 ± 0.03 | 0.09 ± 0.03 |
| $E_V$ (kJ mol$^{-1}$) | *1.0* | *1.0* |
| $\tau_V^{298}$ (ps) | 20 ± 5 | 20 ± 5 |
| $\Delta^2$ ($10^{19}$ s$^{-2}$) | 0.13 ± 0.01 | 0.19 ± 0.01 |

Values in *italics* were fixed in the fitting

## Water exchange rate and rotational dynamics

The water exchange rate, which was determined directly from the $^{17}$O $T_2$ data for Gd(L$_3$), $k_{ex}^{298} = 2.8 \times 10^6$ s$^{-1}$, is in good agreement with water exchange rates reported for similar DO3A monoamide derivative Gd$^{3+}$ complexes [11]. According to the empirical rule that has been observed for a large number of amide derivative Gd$^{3+}$ complexes of 1,4,7,10-tetraazacyclododecane-1,4,7,10-tetraacetic acid (DOTA) or DTPA, the water exchange rate is decreased to about one half or one third by the replacement of each carboxylate by an amide function (Table 3) [11]. An amide group is coordinated less strongly with the lanthanide ion than a carboxylate, the bond distances are longer, and as a consequence, the inner sphere is less crowded in amide than in carboxylate complexes [11]. In dissociatively activated water exchange processes, the steric crowding is of primary importance, i.e., a less tightly

310 K are higher than those at 298 K. This shows that the slow water exchange rate is a limiting factor for this complex. Indeed, the proton relaxivities for Gd(L$_1$) could not be fitted with a $k_{ex}^{298}$ value fixed to that of Gd(L$_3$); a reasonable fit could be obtained only when smaller values were considered. We obtained an acceptable fit for $k_{ex}^{298} = 1.0 \times 10^6$ s$^{-1}$, a value about one third of that determined for Gd(L$_3$) by $^{17}$O NMR measurements (Table 5, Fig. 3c, d).

coordinating ligand disfavors the dissociative activation step, leading to a lower water exchange rate.

The rotational dynamics was assessed directly for both the monomer species and the aggregated state by NMRD measurements. The rotational correlation time calculated from the $^{17}O$ $T_1$ data is an average value, since it has contributions from both the monomer and the aggregated state, which cannot be separated. In addition, one cannot use the Lipari–Szabo treatment to analyze the $^{17}O$ NMR data, since they were acquired at only one magnetic field strength, which does not allow the separation of local and global motions. Nevertheless, $\tau_{RO}^{298}$ calculated from $^{17}O$ $T_1$ data clearly shows slow rotational motion: 601 ps for Gd(L$_3$) at 10 mM concentration versus 77 ps for Gd(DOTA)$^-$ (Table 3). On the other hand, the NMRD of the aggregated form could be analyzed in terms of global and local rotation, and these values characterize directly the micellar state. The rotational correlation times obtained from the NMRD curves for the Gd(L$_1$), Gd(L$_2$), and Gd($_3$) monomers are in accordance with their larger size with respect to Gd(DOTA)$^-$. The small variations between the three systems are also coherent with the increasing size of the side chain and its flexibility. Indeed, the smallest $\tau_{RH}^{298}$ value is determined for Gd(L$_1$), which has the shortest linker between the DO3A unit and the PiB unit. Gd(L$_3$) has the longest linker; however, it is more flexible with the C$_5$ alkyl chain than the benzene derivative L$_2$, which therefore has the highest $\tau_{RH}^{298}$ value. As expected, these rotational correlation times are also in accordance with the monomer relaxivities measured at high field.

For the micellar state (Table 5), the global rotational correlation times are in the range of a few nanoseconds [12.0 and 8.0 ns for Gd(L$_1$) and Gd(L$_3$), respectively], whereas the local rotational correlation times are rather short (approximately 100 ps). The generalized order parameter, $S^2$, also has very low values, implying a large flexibility of the system [38].

## Relaxometric assessment of the interaction of the complexes with HSA and Aβ$_{1–40}$ peptide

When the monomeric form of Gd(L$_x$) binds to Aβ plaques, higher relaxivity is expected, in particular at intermediate fields, since the complex becomes immobilized. Indeed, in the presence of the amyloid peptide Aβ$_{1–40}$ ($c_{Gd} = c_{Aβ_{1–40}}$ = 0.2 mM), the relaxivity of Gd(L$_1$) and Gd(L$_3$) increases considerably at magnetic fields where the effect of slower rotation is most pronounced (80 % increase at 40 MHz). This is interesting for imaging applications, where the amyloid binding specifically contributes to a higher MRI efficiency of the agent. The relaxivity increase could be used to assess the binding affinity of the probe for the
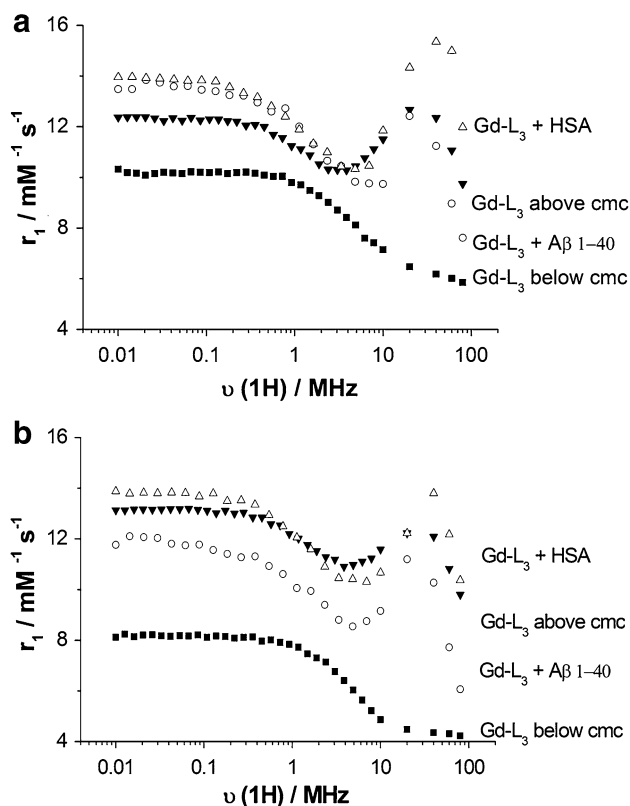


**Fig. 5** $^1H$ NMRD profiles at **a** 298 K and **b** 310 K of Gd(L$_3$) at 0.2 mM (*squares*), 5 mM (*inverted triangles*), 0.2 mM in the presence of 0.2 mM Aβ$_{1–40}$ (*circles*), and 0.2 mM in the presence of 0.2 mM human serum albumin (*HSA*) (*upright triangles*) [0.05 M N-(2-hydroxyethyl)piperazine-N′-ethanesulfonic acid; pH 7.4]. *cmc* critical micellar concentration

amyloid peptide. Instead, amyloid binding affinities for Gd(L$_1$) and Gd(L$_3$) have been investigated in detail by other methods, including surface plasmon resonance and saturation transfer difference NMR, which are more sensitive than relaxometry. These results will be reported elsewhere. The binding affinity of Gd(L$_1$) for Aβ$_{1–40}$, determined from surface plasmon resonance measurements, was published previously ($K_d$ = 180 μM) [20].

Similarly to Gd(L$_1$), Gd(L$_3$) interacts with HSA as well, causing a remarkable increase of relaxivity at intermediate fields (Fig. 5). In general, albumin binding leads to a prolonged lifetime of the agent in the blood pool, which, given the slower elimination from the body, can be useful for an MRI probe. However, strong HSA binding can be detrimental for the BBB permeability of the agent [32].

The binding affinity of Gd(L$_3$) for HSA was assessed by PRE measurements. which are commonly used to determine affinity constants of Gd$^{3+}$ complexes and HSA. The PRE method is a nonseparative technique in which the binding parameters can be obtained by exploiting the differences in the NMR water solvent relaxation rates between the bound and the unbound substrates. Since the
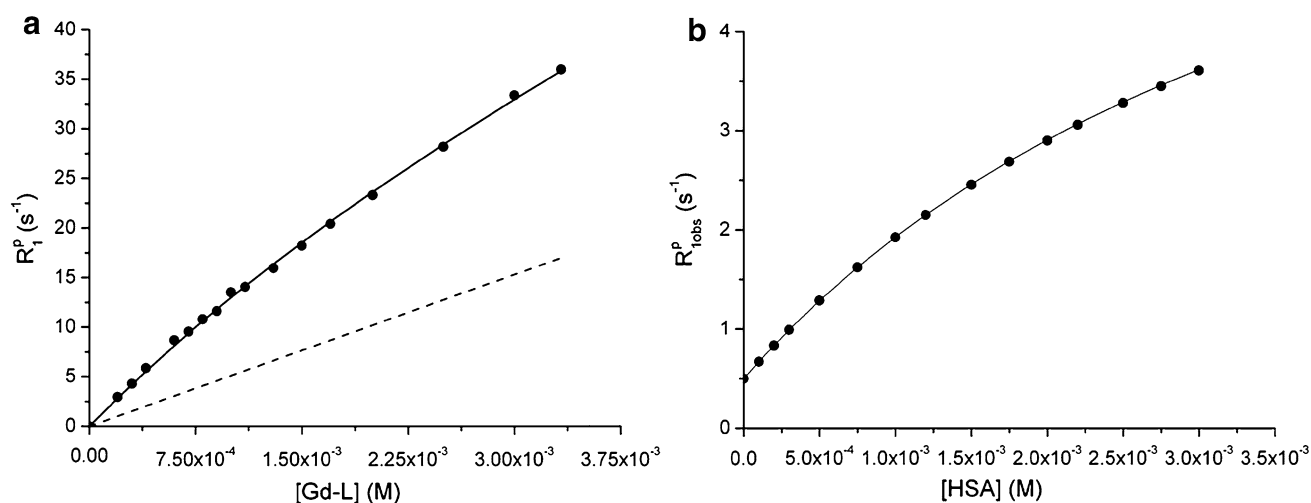
**Fig. 6** Proton relaxation enhancement data to assess HSA binding of Gd(L$_3$): **a** M-titration at 0.6 mM HSA; **b** E-titration at 0.1 mM Gd(L$_3$) (40 MHz, 310 K, pH 7.4)

relaxation rate is markedly increased in the presence of a paramagnetic substrate interacting with the protein, this method is perfectly tailored to investigate the binding of paramagnetic metal chelates. It consists of measuring the proton relaxation rates $R_{1obs}$ at increasing concentrations of the protein and the metal chelate (Fig. 6). To obtain the affinity constant $K_A$, the data were fitted to Eq. 4:

$$R_1^{pobs} = 10^3 \times \left\{ \begin{array}{l} \left(r_1^f \cdot c_1\right) + \frac{1}{2}\left(r_1^c - r_1^f\right) \times \\ \left(nc_{HSA} + c_1 + K_A^{-1} - \sqrt{\left(nc_{HSA} + c_1 + K_A^{-1}\right)^2 - 4nc_{HSA} \cdot C_1}\right) \end{array} \right\}, \tag{4}$$

where $r_1^f$ and $r_1^c$ are the proton relaxivities of the free and the bound state, $c_{HSA}$ and $c_1$ are the concentration of HSA and the complex, respectively, and $n$ is the number of binding sites on the protein.

Under the assumption that there is one binding site in HSA ($n = 1$), a binding constant $K_A$ of $250 \pm 18$ M$^{-1}$,

and a relaxivity of the non-covalently bound complex $r_1^c$ of $77 \pm 5.3$ s$^{-1}$ mM$^{-1}$ were obtained for Gd(L$_3$) in comparison with $K_A = 910$ M$^{-1}$ and $r_1^c = 55.5$ s$^{-1}$ mM$^{-1}$ for Gd(L$_1$) (310 K, 40 MHz) (Table 6) [20]. HSA has multiple binding sites. Among the numerous Gd$^{3+}$ complexes with HSA-binding capability that have been investigated in the past, some were reported to bind to more than one independent site with different binding constants [41, 42]. Typically, these different binding constants are derived from ultrafiltration experiments. Most often, relaxometric data alone do not allow one to distinguish between different binding models. On the other hand, the stepwise binding constants calculated from the ultrafiltration data

**Table 6** Parameters obtained from relaxometric titrations of [Gd(L$_1$)(H$_2$O)] and [Gd(L$_3$)(H$_2$O)] complexes with human serum albumin (40 MHz), compared with literature data for other complexes (310 K)

| Complex | $K_A$ (10$^3$ M$^{-1}$) | $n$ | $r_1^c$ (s$^{-1}$ mM$^{-1}$) | $r_1^f$ (s$^{-1}$ mM$^{-1}$) | References |
|---|---|---|---|---|---|
| Gd(L$_1$) | $0.91 \pm 0.09$ | 1 | $55 \pm 8.6$ | $5.3 \pm 0.2$ | [20] |
| Gd(L$_3$) | $0.25 \pm 0.02$ | 1 | $77 \pm 5.3$ | $4.9 \pm 0.1$ | This work |
| Gd(BOPTA)$^{2-}$ | 1.5 | 1 | 42.9 | 5.2 | [44] |
| MS-325 | 6.1 | 1 | 48.9 | 5.6 | [44] |
| Gd(Bz-DTTA)$^{-}$ | 0.71 | 1 | 45.5 | 7.1 | [45] |

Gd(BOPTA)$^{2-}$, (4RS)-[4-carboxy-5,8,11-tris(carboxymethyl)-1-phenyl-2-oxa-5,8,11-triazatridecan-13-oato(5-)] gadolinate(2-); Bz-DTTA, N′-benzyl-diethylene-triamine-N,N,N″,N″-tetraacetic acid; MS-325, trisodium {(2-(R)-[(4,4-diphenylcyclohexyl) phosphonooxymethyl]-diethylenetriaminepentaacetato)(aquo) gadolinium(III)

typically show that one binding site is much stronger than the others ($K_{a1}/K_{a2}$ between 15 and 30); therefore, a 1:1 binding isotherm is used most commonly for the albumin binding of related $Gd^{3+}$ complexes [43].

Our complexes show moderate binding as compared with $Gd(BOPTA)^{2-}$ or MS-325, which were specifically developed as blood pool agents exhibiting strong HSA binding [44]. The affinity is similar to that determined for $Gd(Bz-DTTA)^-$, a linear DTPA-type chelate bearing a benzyl substituent. We have not found any literature data concerning the binding of the small molecule PiB to HSA.

## Conclusions

We have synthesized a family of metal-based molecular imaging probes for the detection of amyloid plaques associated with AD. The ligands are obtained by linking the PiB moiety, an efficient amyloid marker, to DO3A monoamide, which forms stable and inert complexes with various metal ions adapted to different imaging modalities, including $Gd^{3+}$ for MRI, $^{111}In^{3+}$ for SPECT, or $^{68}Ga^{3+}$ for PET. The ligands differ in the chemical structure and the length of the spacer between the PiB unit and the DO3A unit, which allows hydrophobicity of the complexes to be modulated. The $Gd(L_x)$ chelates have amphiphilic behavior as shown by their octanol–water partition coefficients and form micelles in solution. The cmcs, which were obtained by relaxometric measurements, are in the low millimolar range. The parameters that influence water proton relaxivity, including the water exchange rate and the rotational correlation times, were determined in a combined $^{17}O$ NMR and NMRD study. The analysis of the rotational dynamics for the aggregated micellar state in terms of local and global motions using the Lipari–Szabo approach indicated highly flexible, large aggregates. The $Gd(L_x)$ complexes bind the amyloid peptide $A\beta_{1-40}$ and HSA, yielding increased relaxivities owing to reduced rotational motion. HSA binding affinity constants ($K_A$) of 250 and 910 $M^{-1}$ were calculated for $Gd(L_1)$ and $Gd(L_3)$, respectively, from PRE experiments.

These $Gd^{3+}$ complexes will likely not pass the BBB in sufficient amount for MRI detection. Nevertheless, they might be still useful in animal studies with BBB opening, in intracerebroventricular injection protocols, or in ex vivo MRI to stain AD brain tissues.

## References

1. Fratiglioni L, Winblad B, von Strauss E (2007) Physiol Behav 92:98–104. doi:10.1016/j.physbeh.2007.05.059
2. Hardy J, Selkoe DJ (2002) Science 297:353–356. doi:10.1126/science.1072994
3. Rauk A (2009) Chem Soc Rev 38:2698. doi:10.1039/b807980n
4. Camus V, Payoux P, Barré L et al (2012) Eur J Nucl Med Mol Imaging 39:621–631. doi:10.1007/s00259-011-2021-8
5. Mathis CA, Bacskai BJ, Kajdasz ST, McLellan ME, Frosch MP, Hyman BT, Holt DP, Wang Y, Huang G-F, Debnath ML, Klunk WE (2002) Bioorg Med Chem Lett 12:295–298. doi:10.1016/S0960-894X(01)00734-X
6. Vandenberghe R, Van Laere K, Ivanoiu A, Salmon E, Bastin C, Triau E, Hasselbalch S, Law I, Andersen A, Korner A, Minthon L, Garraux G, Nelissen N, Bormans G, Buckley C, Owenius R, Thurfjell L, Farrar G, Brooks DJ (2010) Ann Neurol 68:319–329. doi:10.1002/ana.22068
7. Barthel H, Gertz H-J, Dresel S, Peters O, Bartenstein P, Buerger K, Hiemeyer F, Wittemer-Rump SM, Seibyl J, Reininger C, Sabri O (2011) Lancet Neurol 10:424–435. doi:10.1016/S1474-4422(11)70077-1
8. Verhoeff NPLG, Wilson AA, Takeshita S, Trop L, Hussey D, Singh K, Kung HF, Kung M-P, Houle S (2004) Am J Geriatr Psychiatry 12:584–595. doi:10.1176/appi.ajgp.12.6.584
9. Nordberg A (2004) Lancet Neurol 3:519–527. doi:10.1016/S1474-4422(04)00853-1
10. Cheng Y, Ono M, Kimura H, Ueda M, Saji H (2012) J Med Chem 55:2279–2286. doi:10.1021/jm201513c
11. Merbach AE, Helm L, Toth E (2013) The chemistry of contrast agents in medical magnetic resonance imaging, 2nd edn. Wiley, New York
12. Jack CR Jr, Garwood M, Wengenack TM, Borowski B, Curran GL, Lin J, Adriany G, Gröhn OHJ, Grimm R, Poduslo JF (2004) Magn Reson Med 52:1263–1271. doi:10.1002/mrm.20266
13. Higuchi M, Iwata N, Matsuba Y, Sato K, Sasamoto K, Saido TC (2005) Nat Neurosci 8:527–533. doi:10.1038/nn1422
14. Poduslo JF, Wengenack TM, Curran GL, Wisniewski T, Sigurdsson EM, Macura SI, Borowski BJ, Jack CR (2002) Neurobiol Dis 11:315–329. doi:10.1006/nbdi 2002.0550
15. Wadghiri YZ, Sigurdsson EM, Sadowski M, Elliott JI, Li Y, Scholtzova H, Tang CY, Aguinaldo G, Pappolla M, Duff K, Wisniewski T, Turnbull DH (2003) Magn Reson Med 50:293–302. doi:10.1002/mrm.10529
16. Poduslo JF, Curran GL, Peterson JA, McCormick DJ, Fauq AH, Khan MA, Wengenack TM (2004) Biochemistry (Mosc) 43:6064–6075. doi:10.1021/bi0359574
17. Yang J, Wadghiri YZ, Hoang DM, Tsui W, Sun Y, Chung E, Li Y, Wang A, de Leon M, Wisniewski T (2011) Neuroimage 55:1600–1609. doi:10.1016/j.neuroimage.2011.01.023
18. Larbanoix L, Burtea C, Laurent S, Van Leuven F, Toubeau G, Elst LV, Muller RN (2010) Neurobiol Aging 31:1679–1689. doi:10.1016/j.neurobiolaging.2008.09.021
19. Solomon I (1955) Phys Rev 99:559. doi:10.1103/PhysRev.99.559
20. Martins AF, Morfin J-F, Kubíčková A, Kubíček V, Buron F, Suzenet F, Salerno M, Lazar AN, Duyckaerts C, Arlicot N, Guilloteau D, Geraldes CFGC, Tóth É (2013) ACS Med Chem Lett 5:436–440. doi:10.1021/ml400042w

21. Vithanarachchi SM, Allen MJ (2013) Chem Commun 49:4148–4150. doi:10.1039/C2CC36583A
22. Barge A, Cravotto G, Gianolio E, Fedeli F (2006) Contrast Media Mol Imaging 1:184–188. doi:10.1002/cmmi.110
23. Leo A, Hansch C, Elkins D (1971) Chem Rev 71:525–616. doi:10.1021/cr60274a001
24. Anthony JL, Maginn EJ, Brennecke JF (2001) J Phys Chem B 105:10942–10949. doi:10.1021/jp0112368
25. Raiford DS, Fisk CL, Becker ED (1979) Anal Chem 51:2050–2051. doi:10.1021/ac50048a040
26. Hugi AD, Helm L, Merbach AE (1985) Helv Chim Acta 68:508–521. doi:10.1002/hlca.19850680224
27. Mathis CA, Wang Y, Holt DP, Huang G-F, Debnath ML, Klunk WE (2003) J Med Chem 46:2740–2754. doi:10.1021/jm030026b
28. Wang Y, Klunk WE, Huang G-F, Debnath ML, Holt DP, Mathis CA (2002) J Mol Neurosci 19:11–16. doi:10.1007/s12031-002-0004-8
29. Thyagarajan BS (1958) Chem Rev 58:439–460. doi:10.1021/cr50021a001
30. Schotten C (1884) Ber Dtsch Chem Ges 17:2544–2547. doi:10.1002/cber.188401702178
31. Baumann E (1886) Ber Dtsch Chem Ges 19:3218–3222. doi:10.1002/cber.188601902348
32. Mensch J, Oyarzabal J, Mackie C, Augustijns P (2009) J Pharm Sci 98:4429–4468. doi:10.1002/jps.21745
33. Lin K-S, Debnath ML, Mathis CA, Klunk WE (2009) Bioorg Med Chem Lett 19:2258–2262. doi:10.1016/j.bmcl.2009.02.096
34. Earnshaw A, Greenwood N (1997) Chemistry of the elements. Elsevier, Amsterdam
35. Levin VA (1980) J Med Chem 23:682–684
36. Bornebroek M, Verzijlbergen JF, Haan J, Van Scheyen EJ, Verhoeff NP, Pauwels EK, Roos RA (1996) Nucl Med Commun 17:929–933
37. Saito Y, Buciak J, Yang J, Pardridge WM (1995) Proc Natl Acad Sci USA 92:10227–10231
38. Nicolle GM, Toth E, Eisenwiener K-P, Mäcke HR, Merbach AE (2002) J Biol Inorg Chem 7:757–769. doi:10.1007/s00775-002-0353-3
39. Powell DH, Dhubhghaill OMN, Pubanz D, Helm L, Lebedev YS, Schlaepfer W, Merbach AE (1996) J Am Chem Soc 118:9333–9346. doi:10.1021/ja961743g
40. Caravan P, Ellison JJ, McMurry TJ, Lauffer RB (1999) Chem Rev 99:2293–2352. doi:10.1021/cr980440x
41. Caravan P, Cloutier NJ, Greenfield MT, McDermid SA, Dunham SU, Bulte JWM, Amedio JC Jr, Looby RJ, Supkowski RM, Horrocks WD Jr, McMurry TJ, Lauffer RB (2002) J Am Chem Soc 124:3152–3162
42. Moriggi L, Yaseen MA, Helm L, Caravan P (2012) Chem Eur J 18:3675–3686. doi:10.1002/chem.201103344
43. Giardiello M, Botta M, Lowe MP (2011) J Incl Phenom Macrocycl Chem 71:435–444. doi:10.1007/s10847-011-0009-4
44. Henrotte V, Vander Elst L, Laurent S, Muller RN (2007) JBIC J Biol Inorg Chem 12:929–937. doi:10.1007/s00775-007-0247-5
45. Silverio S, Torres S, Martins AF, Martins JA, Andre JP, Helm L, Prata MIM, Santos AC, Geraldes CFGC (2009) Dalton Trans 4656–4670